Supporting figures and data

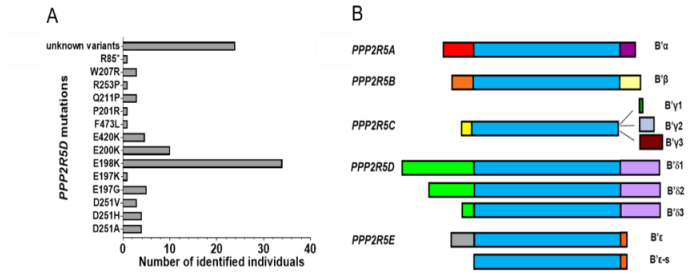

Figure 1. Figure 1. A. The PP2R5D mutations and numbers of patients for each variant of Jordan's Syndrome (data from a year ago). **B**. Cartoon representation of the members of PP2A regulatory subunits in B' family. Colored boxes indicate sequence differences. In addition to a conserved core region (blue box) common to all B' members, it contains unique N and C-terminal extensions of ~100 amino acids each.

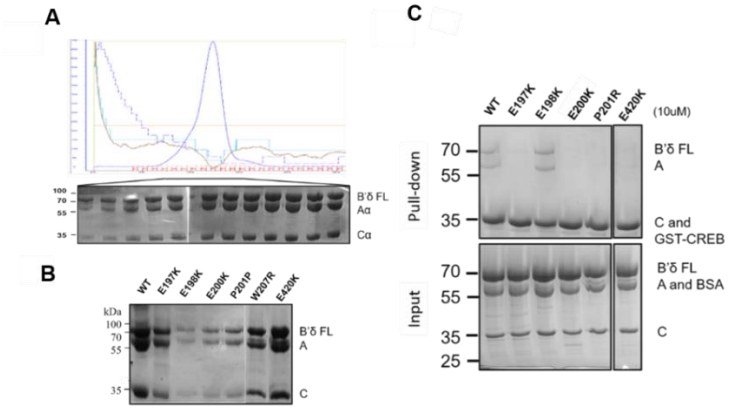

Figure 2. A. Protein preparations of variants of PP2A-B'δ holoenzymes. Each subunit was expressed, purified and assembled with other subunits followed by a size exclusion chromatography. **B.** Complexes analyzed by SDS-PAGE and visualized by Coomassie blue staining. **C.** The pull-down assay using GST-CREB to pull down WT and variants of PP2A-B'δ (10 μM).

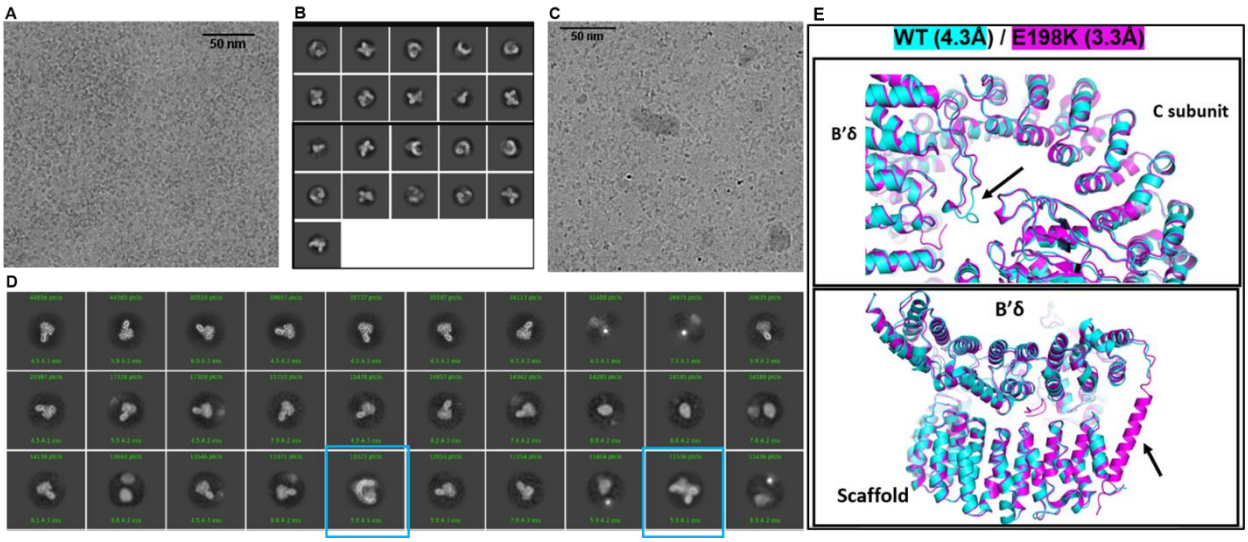

Figure 3. A. Representative micrograph of E198K PP2A-B'δ holoenzyme (home-made grids) collected by Titan Krios with K2 camera at NYSBC. **B.** 2D class averages of E198K holoenzyme. **C.** Representative micrograph of WT PP2A-B'δ holoenzyme (Chameleon grids) collected by Titan Krios with K2 camera at NYSBC. **D.** 2D class averages of WT holoenzyme showing clearly defined subunits in blue highlighted squares. **E.** Superimposition of WT (Cyan) and E198K mutant (magenta) of PP2A-B'δ holoenzymes indicating the differences in B'δ subunit (top) and in the scaffold subunit (bottom).

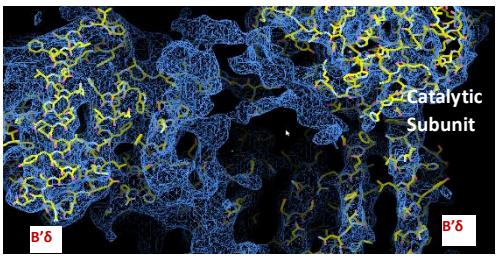

Figure 4. Electron density map and preliminary model for WT holoenzyme from Chameleon grids. The density map for unmodeled regulatory domains is observed between B'δ and catalytic subunits, which makes extensive contacts with the substrate binding pocket and residues changed in disease variants.

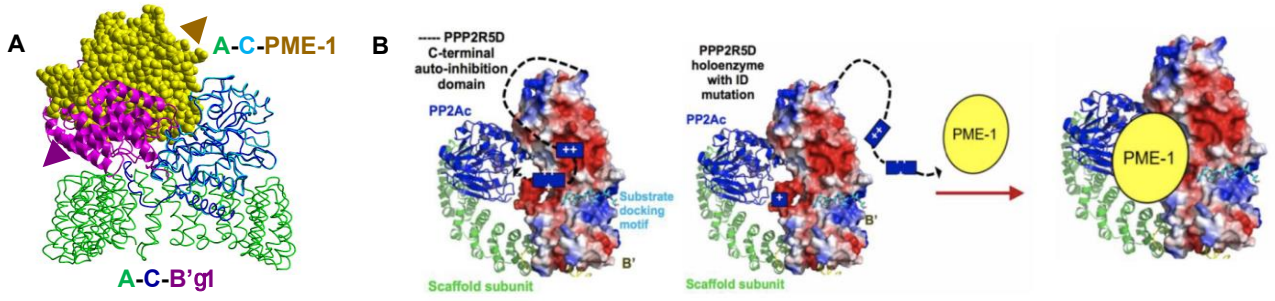

Figure 5. A. Overlay of the structure of the PP2A-B′γ1 holoenzyme (PDB code: 2NPP) to the complex of PME-1 bound to the PP2A core enzyme (PDB code: 3C5W) via the catalytic subunit and the C-terminal five HEAT repeats of the A subunit. The structural alignment illustrates the steric hindrance of regulatory subunits to exclude PME-1 binding to the holoenzymes. **B.** The hypothesized mechanism of PPP2R5D mutation allows the PP2A holoenzyme to be more prone to PP2A**.**

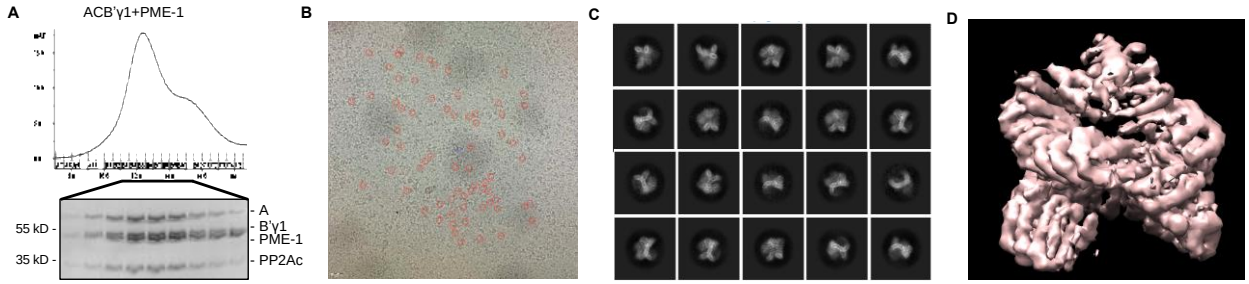

Figure 6. A. PP2A-B' γ1 holoenzyme and PME-1 co-migrated over gel filtration chromatography. Protein fractions were analyzed by SDS-PAGE and visualized by Coomassie blue staining. **B.** The image shows a representative cryo-EM image of PME-1- PP2A-B' γ1 complex particle. Some particles are highlighted with red circles. **C.** Representative 2D class averages. **D.** Low resolution map of PME-1- PP2A-B' γ1 complex.

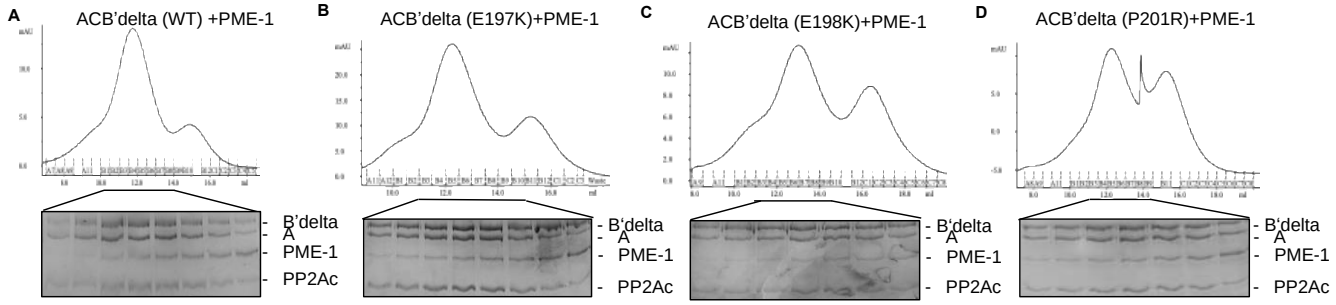

Figure 7. PME-1 and different PP2A-B' δ holoenzymes co-migrated over gel filtration chromatography. Protein fractions were analyzed by SDS-PAGE and visualized by Coomassie blue staining. The data shows that interactions between three mutated PP2A-B' δ holoenzymes and PME-1 were slightly stronger than that of wild-typed PP2A-B' δ holoenzyme, and all four PP2A-B' δ holoenzymes reduced binding to PME-1 compared with PP2A-B' γ1 holoenzyme (Fig S5A).